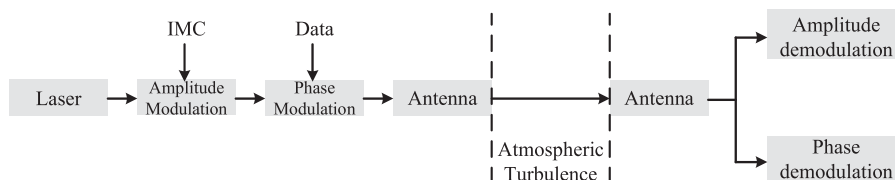


Performance Analysis of IMC in FSO Systems Over Gamma–Gamma Channel

Volume 10, Number 3, June 2018




Tao Shang
Renjie Chen
Yuanhao Liu
Yan Gao



DOI: 10.1109/JPHOT.2018.2842716

1943-0655 © 2018 IEEE

Performance Analysis of IMC in FSO Systems Over Gamma–Gamma Channel

Tao Shang ,^{1,2} Renjie Chen ,^{1,2} Yuanhao Liu,^{1,2} and Yan Gao  ^{1,3}

¹State Key Laboratory of Integrated Service Networks, School of Telecommunications Engineering, Xidian University, Xian 710071, China

²Collaborative Innovation Center of Information Sensing and Understanding, Xidian University, Xian 710071, China

³The Institute of China Electronic System Engineering Corporation, Beijing 100039, China

DOI:10.1109/JPHOT.2018.2842716

1943-0655 © 2018 IEEE. Personal use is permitted, but republication/redistribution requires IEEE permission. See http://www.ieee.org/publications_standards/publications/rights/index.html for more information.

Manuscript received May 6, 2018; revised May 28, 2018; accepted May 29, 2018. Date of publication May 30, 2018; date of current version June 12, 2018. This work is supported in part by the 863 High Technology Plan of China under Grant 2013AA013402 and in part by the National Natural Science Foundation of China under Grants 61172080 and 61771357. Corresponding author: Tao Shang (e-mail: shtsun_sjtu@hotmail.com).

Abstract: Free-space optical communication (FSO) offers high security and high bandwidth, which is why it is widely used in digital communication systems. However, atmospheric turbulence or scintillation induces a voluminous degradation to the signal. So, different modulation techniques are introduced to improve the performance of FSO systems. In this paper, a novel inverted Manchester code (IMC) and a 3 bits-per-symbol modulation format are proposed, referred to as IMC/BPSK. The BERs of the IMC/BPSK amplitude branch and phase branch are studied theoretically and numerically over the gamma–gamma channel model separately, and the capacity is also been studied. The simulation comparison with 8-PPM is also made. The results show that the BER performance of IMC/BPSK is better than that of 8-PPM with the same symbol rate. Therefore, the proposed modulation format is feasible, which can effectively improve the tolerance degree of the atmospheric turbulence effect.

Index Terms: Inverted Manchester code, IMC/BPSK, FSO, gamma-gamma channel model, atmospheric turbulence.

1. Introduction

Free space optical communication (FSO) has been widely deployed for inter-satellite and deep-space communications. In recent years, however, because of its multiple advantages such as extremely high bandwidth, license-free, and interference immunity etc. [1], FSO has attracted considerable attention for a variety of applications, e.g. last mile connectivity [2], optical-fiber backup and enterprise connectivity. In such kind of applications, FSO systems basically utilize atmosphere as transmission medium rather than the free space. So the performance of FSO link is inherently affected by atmospheric conditions. Among these conditions, atmospheric turbulence has the most significant effect. It causes random fluctuations at the received signal intensity, i.e., channel fading, which leads to an increase in the bit error rate (BER) of the optical link.

In order to improve the stability and reliability of FSO systems and weaken the influence of atmospheric turbulence, it is very important to study the suitable modulation technologies. In the FSO systems, intensity modulation with direct detection (IM/DD) is widely used, such as on-off keying (OOK) [3] and pulse-position modulation (PPM) [4], [5]. However, there are also many

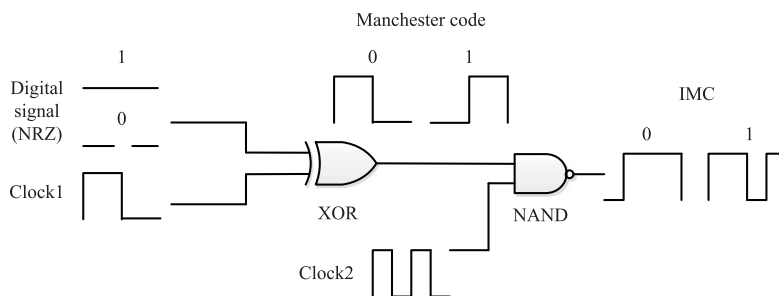


Fig. 1. Generation of IMC signals.

issues, like the lack of power efficiency in OOK and the sacrifice of bandwidth efficiency in PPM. Furthermore, phase-shift keying (PSK) is also an alternative scheme to OOK and PPM [6], [7], and the performance of PSK with pointing errors has been investigated in [8].

In this paper, a novel inverter Manchester code (IMC) is proposed, and then combined with amplitude and phase modulation, a new modulation format of IMC/BPSK is put forward, which is a 3bits-per-symbol modulation format. On this basis, a FSO system based on IMC/BPSK is designed. IMC can be divided into two branches according to its code element: the branch loading the amplitude information is called amplitude branch and the other branch loading the phase information is called phase branch. In such a code, the amplitude branch and phase branch can transmit 1bit and 2bits information respectively, which improves the bit rate of FSO systems. The IMC/BPSK signal propagates through the atmospheric channel, which is modeled as Gamma-Gamma distribution. At receiving end, an avalanche photodiode (APD) is utilized to get photocurrent, and the demodulation progress of amplitude branch and phase branch are separated. Based on this system, the BER formula of amplitude branch and phase branch are derived through Meijer-G function, the channel capacity of IMC/BPSK is also been analysed. To verify our work, the simulations are made. We first get the optimal value of APD gain, which is used to achieve the best BER performance under different turbulence. After obtaining the BER curves of amplitude branch and phase branch, we compare them with 8-PPM under the same condition, the reason is that both IMC and 8-PPM can transmit 3bits information in one symbol. The result shows that IMC/BPSK format is better than 8-PPM in the suppression of the atmospheric turbulence effect.

The rest of the paper is organized as follows: In Section 2, the IMC scheme and a FSO system based on the IMC/BPSK are proposed. In Section 3, the BERs of the IMC/BPSK over Gamma-Gamma channel model are theoretically analyzed, the expressions of BER and capacity are given. Section 4 shows the numerical results of BER performances and the comparison between IMC/BPSK and 8-PPM. Conclusions can be found in Section 5.

2. IMC and the IMC/BPSK Based FSO System

Because of IMC is a novel code that we designed with unique features, and the modulation format IMC/BPSK and the FSO system are all based on the features of it, here we decide to describe the generation and the features of IMC at first. And then we will give the FSO system on the basis of IMC.

Fig. 1 shows the scheme to generate the electrical IMC signal. The NRZ data and a 50% duty cycle Clock 1 (the same frequency as NRZ) first pass through a XOR gate to generate Manchester code, then the generated Manchester code and a 50% duty cycle Clock 2 (twice the frequency of NRZ) pass through a NAND gate to generate IMC signal. And the waveform generation process of IMC signal is shown in Fig. 2. In Fig. 3, there are two varying symbols in IMC signal that represent 0 and 1. Furthermore, the first and third slot vary between 01 and 10, whereas the second and fourth slot always keep constant. So we utilize this characteristic to modulate the amplitude information

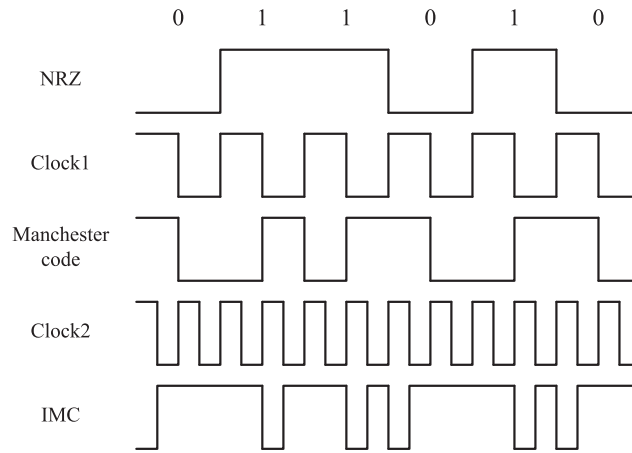


Fig. 2. Waveform generation process of IMC signal.

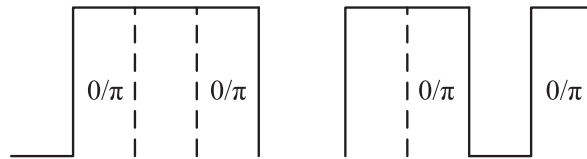


Fig. 3. Symbols of IMC.

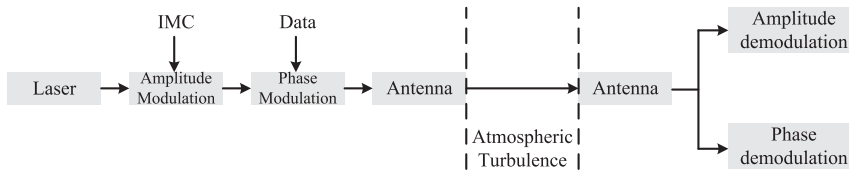


Fig. 4. Schematic diagram of FSO system based on the IMC/BPSK modulation format.

on the first and third slot, which is referred to as amplitude branch, and we modulate the phase information on the second and fourth slot, which is referred to as phase branch.

Fig. 4 shows the FSO system based on the IMC/BPSK modulation format. The laser beam is externally modulated by electrical IMC signal with certain rate to generate the optical IMC signal. A phase modulator is used to overlay on the IMC signal with two times rate BPSK signal, so the IMC/BPSK signal is generated. Then this signal is launched by the antenna. At the receiving end, the optical power is divided into two branches to demodulate the information of the amplitude and the phase respectively.

3. The Performance of IMC/BPSK

3.1 Gamma-Gamma Channel Model

The Gamma-Gamma distribution is suitable for both weak and strong turbulence [9], so we use it in the analysis. The probability density function (PDF) of a random variable K_s is given by [10]

$$f(K_s) = \frac{2(\alpha\beta)^{\frac{\alpha+\beta}{2}}}{\Gamma(\alpha)\Gamma(\beta)\overline{K_s}} \left(\frac{K_s}{\overline{K_s}}\right)^{\frac{\alpha+\beta}{2}-1} \times K_{\alpha-\beta} \left(2\sqrt{\frac{\alpha\beta K_s}{\overline{K_s}}}\right) \quad (1)$$

where $K_c(\cdot)$ is the c th-order modified Bessel function of the second kind, $\Gamma(\cdot)$ is the Gamma function, α and β represent the large and small scale optical wave intensity, which are related to scintillation index, and $\overline{K_s}$ is the mean value of the random variable K_s .

Assuming plane wave propagation, α and β can thus directly be linked to physical parameters and represented by [10]

$$\alpha = \left[\exp \left(\frac{0.49\sigma_R^2}{(1 + 1.11\sigma_R^{\frac{12}{5}})^{\frac{7}{6}}} \right) - 1 \right]^{-1} \quad (2)$$

$$\beta = \left[\exp \left(\frac{0.51\sigma_R^2}{(1 + 0.69\sigma_R^{\frac{12}{5}})^{\frac{5}{6}}} \right) - 1 \right]^{-1} \quad (3)$$

where α and β are the scintillation parameters depending on the Rytov variance σ_R^2 , which is for plane wave propagation expressed as [10]

$$\sigma_R^2 = 1.23C_n^2 k_w^{\frac{7}{6}} L^{\frac{11}{6}} \quad (4)$$

In (4), C_n^2 is the strength of the atmospheric turbulence, L is the propagation distance, $k_w = 2\pi/\lambda$ is the optical wave number, where λ is the wavelength. In general, C_n^2 ranges from $10^{-13}m^{-2/3}$ for strong turbulence to $10^{-17}m^{-2/3}$ for weak turbulence [11]. The scintillation index is related to α and β as

$$\mathcal{X}_{sc} = \frac{1}{\alpha} + \frac{1}{\beta} + \frac{1}{\alpha\beta} \quad (5)$$

3.2 Amplitude Branch

For the amplitude branch, the demodulation pattern is direct detection. For a high bit rate optical communications, APD is frequently the photodetector of choice due to its internal gain, which provides better sensitivity and fast response times than PIN photodiode [12]. Here we use Si-APD in the FSO system. For an APD detector, the noise mainly consists of thermal noise and shot noise produced by signal current and dark current. In general, the value of dark current is quite small, which is negligible. In the case of ignoring the dark current, the photocurrent received at the receiving end can be expressed as [13]

$$x(t) = e \sum_{n=-\infty}^{\infty} g_n h(t - t_n) + n(t) \quad (6)$$

where e is electron charge, g_n is the random gain of APD, $h(t)$ is response function, t_n is response time, $n(t)$ is the thermal noise whose power spectral density is $2kT_0/R_L$, k is the Boltzmann constant, T_0 is the absolute temperature at the receiver, and R_L is the load resistance of APD.

Because the statistical process of photoelectric detection is Poisson process, the received light intensity can be represented by the number of the received photons [14]

$$\lambda_r(t) = \lambda_b + \lambda_s(t)d(t) \quad (7)$$

where $\lambda_r(t)$ denotes the average photon number received per time unit, λ_b is the average photon number received caused by background light noise, and $\lambda_s(t)$ is the instantaneous photon number received under the effects of atmospheric turbulence.

In fact, because of the IMC slot is very short and the change of atmospheric scintillation is normally slow, we therefore can assume that the scintillation is fixed in an IMC slot, so $\lambda_s(t)$ is constant, and it is expressed as [14]

$$\lambda_s = \frac{\eta A_d I}{2h\nu} \quad (8)$$

where η is quantum efficiency of the detector, A_d is the area of the receiving aperture, I is the received irradiance of light, h is Planck constant, and ν is the frequency of light waves.

According to (7), both λ_s and I are random variables consistent with Gamma distribution. So the conditional bit error rate of amplitude branch can be expressed as [15]

$$P_{b|\gamma_{amp}} = Q(\sqrt{\gamma_{amp}}) \quad (9)$$

where γ_{amp} is the signal-to-noise ratio (SNR) of the receiving end [14]

$$\gamma_{amp} = \frac{(\bar{g}e)^2 K_s^2}{(\bar{g}e)^2 F(K_s + 2K_b) + 2\sigma_n^2} \quad (10)$$

where $Q(x)$ is expressed as [16]

$$Q(x) = \frac{1}{2\pi} \int_x^\infty \exp\left(-\frac{y^2}{2}\right) dy \quad (11)$$

where $\bar{g} = E(g_n)$ denotes the average gain of APD, e denotes electron charge, $K_b = \lambda_b T_w / 4$ denotes the average background noise photon count per IMC slot, $K_s = \lambda_s T_w / 4$ denotes the received photon per IMC slot, T_w denotes the symbol period, $F = (E(g_n^2) / \bar{g}^2)$ denotes the noise factor of APD, and $\sigma_n^2 = (2kT_0 / R_L)(T_w / 4)$ denotes the thermal noise at the receiver per IMC slot. The noise factor F is represented by [14]

$$F = \zeta \bar{g} + \left(2 - \frac{1}{\bar{g}}\right) (1 - \zeta) \quad (12)$$

where ζ is the ionization factor.

Simplify (10),

$$\gamma_{amp} = \frac{K_s^2}{FK_s + K_n} \quad (13)$$

$$K_n = \left(\frac{2\sigma_n^2}{(\bar{g}e)^2}\right) + 2FK_b \quad (14)$$

According to the above formulations, and considering the channel coefficient and the noise are independent, the BER of the amplitude branch is expressed as [14]

$$P_{amp} = \int_0^\infty Q(\sqrt{\gamma_{amp}}) f(K_s) dK_s \quad (15)$$

In order to provide a closed-form solution of the above integral, we express the $K_c(\cdot)$ and $\text{erfc}(\cdot)$ function in terms of the Meijer-G function, which can be expressed as [17]

$$K_c(\sqrt{z}) = \frac{1}{2} G_{0,2}^{2,0} \left(\frac{z}{4} \middle|_{c/2, -c/2}^- \right) \quad (16)$$

$$Q(z) = \frac{1}{2} \text{erfc} \left(\frac{\sqrt{2z}}{2} \right) \quad (17)$$

$$\text{erfc}(z) = \frac{1}{\sqrt{\pi}} G_{1,2}^{2,0} \left(z^2 \middle|_{0, 1/2}^1 \right) \quad (18)$$

Then the BER of the amplitude branch is derived by substituting (1), (16), (17), (18) into (15), i.e.,

$$P_{amp} = \frac{(\alpha\beta)^{\frac{\alpha+\beta}{2}}}{2\sqrt{\pi}\Gamma(\alpha)\Gamma(\beta)\bar{K}_s} \int_0^\infty \left(\frac{K_s}{\bar{K}_s}\right)^{\frac{\alpha+\beta}{2}-1} G_{0,2}^{2,0} \left(\alpha\beta \frac{K_s}{\bar{K}_s} \middle|_{(\alpha-\beta)/2, (\beta-\alpha)/2}^- \right) \\ \times G_{1,2}^{2,0} \left(\frac{K_s^2}{2FK_s + 2K_n} \middle|_{0, 1/2}^1 \right) dK_s \quad (19)$$

Finally, using the integral form for the Meijer-G function [18], which is given in Appendix, we get a closed-form solution for the BER of the amplitude branch, which is derived as

$$P_{amp} = \frac{2^{\alpha+\beta-3}}{\pi^{3/2}\Gamma(\alpha)\Gamma(\beta)} G_{5,2}^{2,4} \left(\frac{8K_s^2}{\alpha^2\beta^2(FK_s + K_n)} \middle| \begin{matrix} (1-\beta)/2, (2-\beta)/2, (1-\alpha)/2, (2-\alpha)/2, 1 \\ 0, 1/2 \end{matrix} \right) \quad (20)$$

3.3 Phase Branch

For the phase branch, the demodulation pattern is heterodyne detection, where the received signal is combined with a local oscillator laser. Then the photodetector detects the mixed optical signal to generate the photocurrent. In the case of neglecting atmospheric turbulence, the total power of the mixed signal can be expressed as [19]

$$P = P_S + P_{LO} + 2\sqrt{P_S P_{LO}} \cos[\omega_{IF}t + \theta(t)] \quad (21)$$

where P_S and P_{LO} are the power of the received signal and the power of the local oscillator laser, $\omega_{IF} = \omega_S - \omega_{LO}$ is the angular frequency of intermediate frequency signal, and $\theta(t)$ is phase modulated signal.

For BPSK, $\theta(t)$ takes 0 and π to represent 0 and 1. Then, the output of the APD photodetector can be written as

$$I(t) = \bar{g}R(P_S + P_{LO}) + 2\bar{g}R\sqrt{P_S P_{LO}} \cos[\omega_{IF}t + \theta(t)] + n(t) \quad (22)$$

where R is the responsivity of the receiver, \bar{g} is the average APD gain, and $n(t)$ is the noise combined with the shot noise $i_{Sh}(t)$ and the thermal noise $i_{Th}(t)$. After filtering the DC component, the output electrical signal is given by

$$i(t) = 2\bar{g}R\sqrt{P_S P_{LO}} \cos[\omega_{IF}t + \theta(t)] + i_{Sh}(t) + i_{Th}(t) \quad (23)$$

The shot noise $i_{Sh}(t)$ is generated by the received signal and the local oscillator laser with a power spectral density (PSD) of $N = 2e\bar{g}^2FR(P_{LO} + P_S)$, where e is electron charge, and F is the noise factor of APD. The thermal noise $i_{Th}(t)$ is a zero-mean stationary Gaussian random process, where PSD is $4kT/R_L$, k denotes the Boltzmann constant, T denotes the receiver temperature in Kelvin, and R_L denotes the APDs load resistance.

So the SNR in the case of neglecting atmospheric turbulence can be written by

$$\gamma_{ph} = \frac{|2\bar{g}R\sqrt{P_S P_{LO}}|^2}{2e\bar{g}^2R(P_S + P_{LO})FB + 4kTB/R_L} \quad (24)$$

where B denotes the effective noise bandwidth, and we use $B = R_b/2$, where R_b is the bit rate. It is noted that in a heterodyne detection pattern, if the power of the local oscillator laser P_{LO} is much higher than that of the received signal P_S , the shot noise caused by the received signal and even the thermal noise could be neglected [20]. So we remove the parts of $2e\bar{g}^2RP_SFB$ and $4kTB/R_L$, which denote the power of shot noise caused by the received signal and the power of thermal noise. Then simplify (24),

$$\gamma_{ph} = \frac{2RP_S}{eFB} \quad (25)$$

In order to discuss the phase branch and the amplitude branch under the same conditions, an equivalent transformation $P_S = 4K_s h\nu/T_w$ is utilized, where K_s denotes the received photon per IMC slot, $h\nu$ denotes the energy of a photon, and T_w denotes the IMC symbol period. Then the SNR can be eventually written as

$$\gamma_{ph} = \frac{2RK_s h\nu}{eF} \quad (26)$$

The conditional BER of BPSK is represented as [15]

$$P_b(K_s) = \frac{1}{2} \operatorname{erfc} \left(\sqrt{\frac{\gamma_{ph}}{2}} \right) \quad (27)$$

where $\operatorname{erfc}(\cdot)$ is the complementary error function. Since the bit rate is high enough, we can assume that the change of scintillation is very slow. Thus, the average BER of phase branch can be expressed by [21]

$$P_{phase} = \int_0^\infty P_b(K_s) f(K_s) dK_s \quad (28)$$

Then we obtain the expression for the average BER of phase branch by substituting (1), (27) into (28), and replacing $\operatorname{erfc}(\cdot)$ and $K_c(\cdot)$ by Meijer G-function, which is derived as

$$P_{phase} = \frac{(\alpha\beta)^{\frac{\alpha+\beta}{2}}}{2\sqrt{\pi}\Gamma(\alpha)\Gamma(\beta)\bar{K}_s} \int_0^\infty \left(\frac{K_s}{\bar{K}_s} \right)^{\frac{\alpha+\beta}{2}-1} G_{0,2}^{2,0} \left(\alpha\beta \frac{K_s}{\bar{K}_s} \middle|_{(\alpha-\beta)/2, (\beta-\alpha)/2} \right) \times G_{1,2}^{2,0} \left(\frac{RK_s h\nu}{eF} \middle|_{0,1/2} \right) dK_s \quad (29)$$

Using the integral formula for Meijer-G function that is given in Appendix, the closed-form expression for the average BER of phase branch is deduced as

$$P_{phase} = \frac{1}{2\sqrt{\pi}\Gamma(\alpha)\Gamma(\beta)} G_{3,2}^{2,2} \left(\frac{R\bar{K}_s h\nu}{eF\alpha\beta} \middle|_{0,1/2}^{1-\alpha, 1-\beta, 1} \right) \quad (30)$$

3.4 Channel Capacity

In order to evaluate the performance of the system more comprehensively, we study the capacity of IMC/BPSK in this section. Before evaluating the channel capacity, several assumptions are required. First, the channel is assumed to be uncorrelated [22]. Second, the channel is assumed to be memoryless, stationary and ergodic, with independent and identically distributed intensity fast fading statistics [23].

According to Shannon theorem, the channel capacity is related to the instantaneous electrical SNR, which is referred to as γ . In case of turbulent atmosphere, the PDF of γ can be written as [24]

$$f_\gamma(\gamma) = \frac{(\alpha\beta)^{\frac{\alpha+\beta}{2}}}{\Gamma(\alpha)\Gamma(\beta)\bar{\gamma}} \left(\frac{\gamma}{\bar{\gamma}} \right)^{\frac{\alpha+\beta}{4}-1} \times K_{\alpha-\beta} \left(2\sqrt{\alpha\beta} \sqrt{\frac{\gamma}{\bar{\gamma}}} \right) \quad (31)$$

where $\bar{\gamma}$ denotes the average electrical SNR.

Then the channel capacity with atmospheric turbulence-induced fading can be expressed as [24]

$$C = B \int_0^\infty \log_2(1 + \gamma) f_\gamma(\gamma) d\gamma \quad (32)$$

where B denotes the bandwidth.

Substituting the SNR of amplitude branch and phase branch into (32), the capacity of these two branches can be obtained.

$$C_{amp} = \frac{B_{amp} (\alpha\beta)^{\frac{\alpha+\beta}{2}}}{\Gamma(\alpha)\Gamma(\beta)\bar{\gamma}_{amp} \ln(2)} \int_0^\infty \ln(1 + \gamma_{amp}) \left(\frac{\gamma_{amp}}{\bar{\gamma}_{amp}} \right)^{\frac{\alpha+\beta}{4}-1} K_{\alpha-\beta} \left(2\sqrt{\alpha\beta} \sqrt{\frac{\gamma_{amp}}{\bar{\gamma}_{amp}}} \right) d\gamma_{amp} \quad (33)$$

$$C_{ph} = \frac{B_{ph} (\alpha\beta)^{\frac{\alpha+\beta}{2}}}{\Gamma(\alpha)\Gamma(\beta)\bar{\gamma}_{ph} \ln(2)} \int_0^\infty \ln(1 + \gamma_{ph}) \left(\frac{\gamma_{ph}}{\bar{\gamma}_{ph}} \right)^{\frac{\alpha+\beta}{4}-1} K_{\alpha-\beta} \left(2\sqrt{\alpha\beta} \sqrt{\frac{\gamma_{ph}}{\bar{\gamma}_{ph}}} \right) d\gamma_{ph} \quad (34)$$

where B_{amp} and B_{ph} denote the bandwidth of amplitude branch and phase branch, $\bar{\gamma}_{amp}$ and $\bar{\gamma}_{ph}$ denote the average electrical SNR of the amplitude branch and the phase branch.

In order to make (33), (34) more tractable, (16) and the following formula are used for expressing $K_c(\cdot)$ and $\ln(1 + \gamma)$ by Meijer-G function [23].

$$\ln(1 + z) = G_{1,2}^{2,2} \left(z \middle|_{1,0}^{1,1} \right) \quad (35)$$

Then we can obtain the closed-form expression of capacity under gamma-gamma modeled channel by simplifying the results of last step, where (39) is utilized.

$$C_{amp} = \frac{B_{amp}(\alpha\beta)^{\frac{\alpha+\beta}{2}}}{4\pi \ln(2)\Gamma(\alpha)\Gamma(\beta)\bar{\gamma}_{amp}^{\frac{\alpha+\beta}{4}}} G_{2,6}^{6,1} \left(\frac{(\alpha\beta)^2}{16\bar{\gamma}_{amp}} \middle|_{\frac{\alpha-\beta}{4}, \frac{\alpha-\beta+2}{4}, \frac{\beta-\alpha}{4}, \frac{\beta-\alpha+2}{4}, -\frac{\alpha+\beta}{4}, -\frac{\alpha+\beta}{4}}^{-\frac{\alpha+\beta}{4}, 1-\frac{\alpha+\beta}{4}} \right) \quad (36)$$

$$C_{ph} = \frac{B_{ph}(\alpha\beta)^{\frac{\alpha+\beta}{2}}}{4\pi \ln(2)\Gamma(\alpha)\Gamma(\beta)\bar{\gamma}_{ph}^{\frac{\alpha+\beta}{4}}} G_{2,6}^{6,1} \left(\frac{(\alpha\beta)^2}{16\bar{\gamma}_{ph}} \middle|_{\frac{\alpha-\beta}{4}, \frac{\alpha-\beta+2}{4}, \frac{\beta-\alpha}{4}, \frac{\beta-\alpha+2}{4}, -\frac{\alpha+\beta}{4}, -\frac{\alpha+\beta}{4}}^{-\frac{\alpha+\beta}{4}, 1-\frac{\alpha+\beta}{4}} \right) \quad (37)$$

Since the demodulation of the two branches are respective, the channels of them can be considered as two subchannels of a shared channel, whose capacity is the sum of all the capacity of subchannels. So we can obtain the total IMC/BPSK capacity as $C_{IMC} = C_{amp} + C_{ph}$. Moreover, since the amplitude branch carries 1bit per symbol and the phase branch carries 2bits per symbol, which is mentioned in Section 2, the data rate of the phase branch is two times more than the data rate of the amplitude branch. However, each IMC symbol contains one amplitude symbol and two phase symbols, so the bandwidth of them must be the same, where $B_{amp} = B_{ph} = 1/2B_{IMC}$. Then the capacity of IMC/BPSK can be obtained by substituting (13) and (26) in (36) and (37).

$$C_{IMC} = \frac{B_{IMC}(\alpha\beta)^{\frac{\alpha+\beta}{2}}}{8\pi \ln(2)\Gamma(\alpha)\Gamma(\beta)} \left(\left(\frac{K_s^{-2}}{FK_s + K_n} \right)^{-\frac{\alpha+\beta}{4}} \right. \\ \times G_{2,6}^{6,1} \left(\frac{(\alpha\beta)^2 FK_s + K_n}{16K_s^{-2}} \middle|_{\frac{\alpha-\beta}{4}, \frac{\alpha-\beta+2}{4}, \frac{\beta-\alpha}{4}, \frac{\beta-\alpha+2}{4}, -\frac{\alpha+\beta}{4}, -\frac{\alpha+\beta}{4}}^{-\frac{\alpha+\beta}{4}, 1-\frac{\alpha+\beta}{4}} \right) \\ \left. + \left(\frac{2RK_s h\nu}{eF} \right)^{-\frac{\alpha+\beta}{4}} G_{2,6}^{6,1} \left(\frac{(\alpha\beta)^2 eF}{32RK_s h\nu} \middle|_{\frac{\alpha-\beta}{4}, \frac{\alpha-\beta+2}{4}, \frac{\beta-\alpha}{4}, \frac{\beta-\alpha+2}{4}, -\frac{\alpha+\beta}{4}, -\frac{\alpha+\beta}{4}}^{-\frac{\alpha+\beta}{4}, 1-\frac{\alpha+\beta}{4}} \right) \right) \quad (38)$$

4. Numerical and Results Analysis

In this section, using the above derived formulations, we can estimate the BERs of the IMC amplitude branch and phase branch over atmospheric turbulence channels. In all the numerical analysis below, the system parameters we set are listed in Table 1 [8], [14], where λ , T , R , e , k , h are from [8], K_b , ν , R_L are from [14], others are set as the average level.

Fig. 5 depicts the BER evolution of the amplitude branch in terms of average APD gain \bar{g} for different levels of the received photons per IMC slot, where the temperature is 300K. For analysing the impacts of the scintillation index and the average APD gain on BER, we set χ_{SC} for 0.25, 0.4 and 0.7. It can be seen that the BER decreases first and then increases with the increasing of \bar{g} , so there exists an optimal value of \bar{g} . This is because APD amplifies the signal and noise at the same time. When \bar{g} is relatively small, the signal amplification dominates, and the BER value decreases when \bar{g} increases. But when \bar{g} exceeds the optimal value, the noise amplification dominates, so the BER begins to increase. When focusing on the increase of the scintillation index, the reduction in the optimal APD gain can be found clearly. This means that the effect of increasing the APD gain is relatively small under the circumstance of strong turbulence. Moreover, for a certain gain,

TABLE 1
System Parameters and Constants

Parameters	Symbol	Value
Wavelength	$\lambda(nm)$	1550
Symbol period	$T_w(s)$	$1 * 10^{-9}$
Average background noise photon count per IMC slot	K_b	10
Ionization factor	ζ	0.028
Load resistance	$R_L(\Omega)$	50
Quantum efficiency	η	0.8
Temperature	$T(K)$	300
Distance	$L(km)$	3
Responsivity	$R(A/W)$	1
Electron charge	$e(C)$	$1.6 * 10^{-19}$
Boltzmann constant	$k(W/K/Hz)$	$1.38 * 10^{-23}$
Planck constant	$h(J * s)$	$6.63 * 10^{-34}$

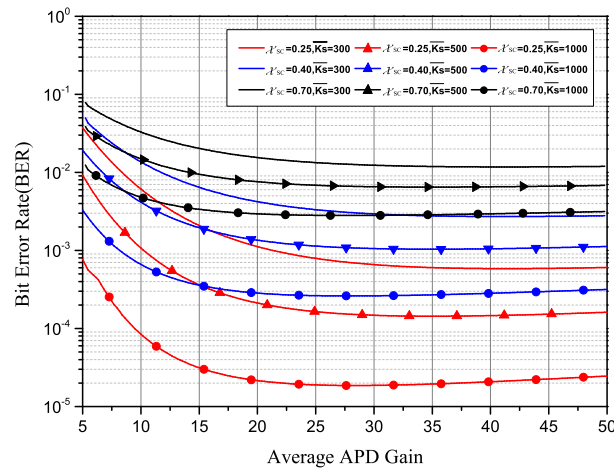


Fig. 5. BER curves of the IMC amplitude branch in terms of APD gain for different \overline{K}_s and λ_{sc} .

the more photons received in an IMC slot, which means the higher received power, the better BER performance will be.

The BER of amplitude branch versus \overline{K}_s is plotted in Fig. 6 for various levels of scintillation index, which gives the impact of the scintillation index on performance. As expected, the BER performance becomes worse with the increase of atmospheric turbulence. It can be seen that it is useful to achieve the same BER performance by increasing the signal power under the weak turbulence scenario. But the effect is gradually weakening when the atmospheric turbulence is strong.

Fig. 7 shows the phase branch BER versus the average APD gain for various levels of scintillation index. It can be seen that the BER performance becomes worse with the increase of average APD gain, which is fairly different from the amplitude branch. This is because we neglect the thermal noise and the shot noise caused by the received signal in the process of computing SNR. So the shot noise caused by local oscillator laser grows faster than the received signal with the increase of average APD gain, which results in the deterioration of BER.

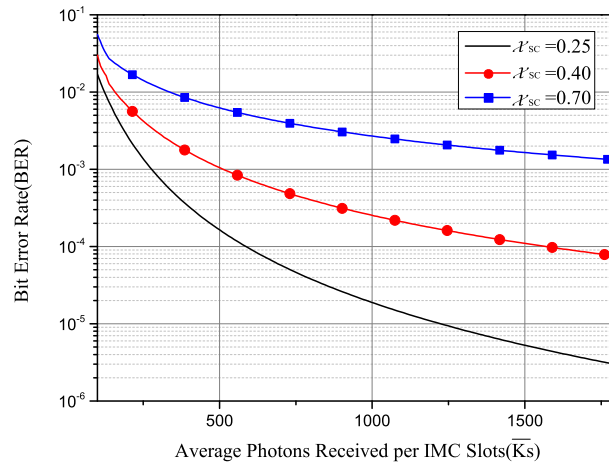


Fig. 6. BER curves of the IMC amplitude branch in terms of \bar{K}_s for different scintillation index.

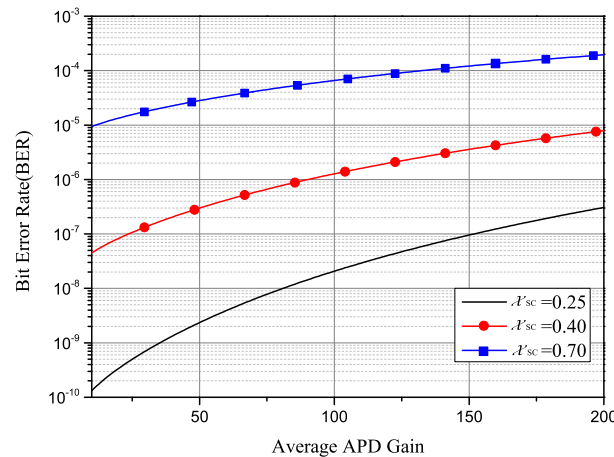


Fig. 7. BER curves of the IMC phase branch in terms of average APD gain for different scintillation index.

Fig. 8 depicts the evolution of phase branch BER in terms of the received photons per IMC slot for various levels of scintillation index, where the average gain of APD is set as the optimal value. It can be seen that the BER decreases with the increase of the received photon number and the decrease of scintillation index. When \bar{K}_s is set as 1000 and the scintillation index is set as 0.70, which represents the strong turbulence, the BER of the phase branch can reach 10^{-5} . Compared with the amplitude branch in the same condition, the BER performance of phase branch is significantly better.

Fig. 9 represents a comparative illustration about the amplitude branch and phase branch of IMC/BPSK and 8-PPM. The BER performance is plotted versus the average received photons per IMC slot under Gamma-Gamma distribution. The scintillation index is set as 0.25 and 0.70, which represent the weak and strong turbulence. Correspondingly, the average gain of APD is 20 and 18.

Fig. 9 clearly shows that when \mathcal{X}_{sc} increases, all the BERs of the amplitude branch, the phase branch and 8-PPM worsen. And when K_s increases, the BERs become better, however, the effect is diminishing. That means the atmospheric turbulence will deteriorate the BER performance, while increasing the number of received photons will have a positive effect on it.

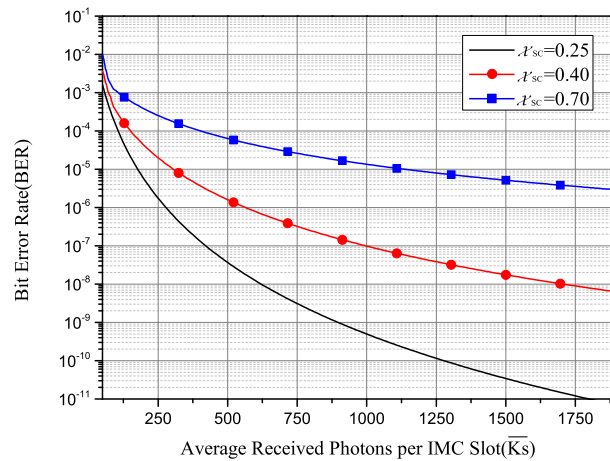


Fig. 8. BER curves of the IMC phase branch in terms of \bar{K}_s for different scintillation index.

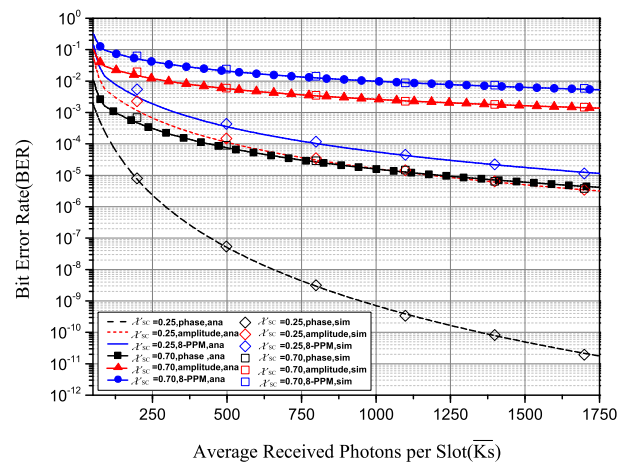


Fig. 9. BER curves of the IMC/BPSK and the 8-PPM.

Fig. 9 also shows that the BER performance of the phase branch is much better than that of the amplitude branch and 8-PPM, which is the same as we expected. As the main effect of the turbulence is intensity scintillation, and its influence on amplitude is more serious than that of the phase. So the signal that is modulated by phase modulation has better BER performance with the same data rate and received signal power. It can be also seen that the BER of amplitude branch is a bit lower than that of 8-PPM, which is because the amplitude branch of the IMC can also be considered as 2-PPM modulation, and there is a feature in M-PPM modulation that is the higher values of M , the worse BER performance will be [25]. Considering the BERs performance of the two branches, it can be concluded that the performance of IMC/BPSK is better than that of 8-PPM in terms of adaptation to atmospheric turbulence.

Fig. 10 shows the comparison between the average channel capacity of IMC/BPSK and 8-PPM under gamma-gamma modeled channel, where χ_{sc} is set as 0.25 and 0.7, and other parameters are set from Table 1. The average channel capacity is the result of C/B , which represents the information transmission capacity of unit bandwidth. Fig. 10 shows that the average channel capacity decreases with the enhancement of scintillation index, which explains the effect of atmospheric turbulence on channel capacity. It can be clearly seen that the average channel capacity is higher than that of 8-PPM, which also means the bandwidth efficiency of IMC/BPSK is better. It is mentioned that the

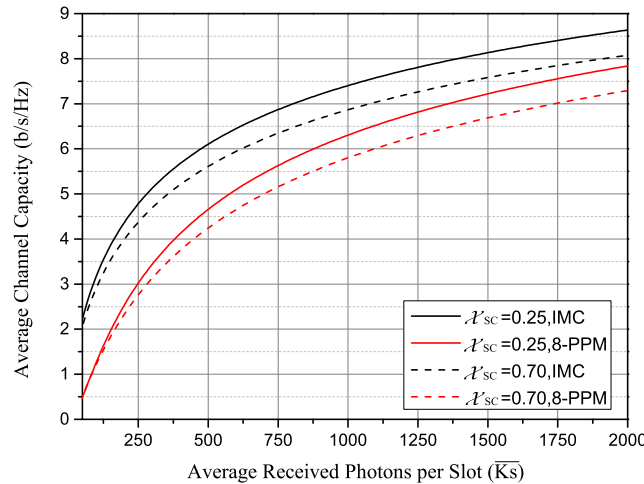


Fig. 10. Average channel capacity curves of the IMC/BPSK and the 8-PPM.

IMC/BPSK and 8-PPM both carry 3bits data per symbol, however there are only 4 slots in an IMC symbol that is less than 8 slots in 8-PPM, so the channel capacity of IMC/BPSK must be higher than that of 8-PPM, when their bandwidths are equal. On the contrary, the bandwidth of IMC/BPSK must be lower than the bandwidth of 8-PPM with the same data rate.

5. Conclusion

In this paper, a novel IMC and a new modulation/demodulation format IMC/BPSK are proposed. Based on the format, the BER performances of FSO systems over Gamma-Gamma distribution models have been studied. The IMC/BPSK is generated by combining amplitude modulation and phase modulation, and this modulation format is 3bits-per-symbol scheme, which can obviously improve the system capacity. In the demodulation scheme, an APD detector is used to improve the systems performance. The amplitude branch is direct detection and the phase branch is heterodyne detection. In order to evaluate the performance of the IMC/BPSK, the BERs of the amplitude branch and phase branch over Gamma-Gamma distribution are deduced, respectively. The expression of channel capacity under turbulent channel is given. The analytical work has been verified by Monte Carlo simulations. The results shows that both the amplitude and phase branch can effectively degrade the impact of atmospheric turbulence. Finally, a comparison between IMC/BPSK and 8-PPM is presented, and the results show that the performances of IMC/BPSK are much better than that of 8-PPM under the same levels of turbulence.

Appendix

In this appendix, we give the integral formula for Meijer-G function [17], which is utilized to get (19) and (28).

$$\int_0^\infty \tau^{\alpha-1} G_{u,v}^{s,t} \left(\sigma \tau \left| \begin{matrix} c_1, \dots, c_t, c_{t+1}, \dots, c_u \\ d_1, \dots, d_s, d_{s+1}, \dots, d_v \end{matrix} \right. \right) G_{p,q}^{m,n} \left(\omega \tau^{l/k} \left| \begin{matrix} a_1, \dots, a_n, a_{n+1}, \dots, a_p \\ b_1, \dots, b_m, b_{m+1}, \dots, b_q \end{matrix} \right. \right) d\tau = \frac{k^\mu \Gamma(v-u)\alpha + \rho - 1}{(2\pi)^{(l-1)b^* + (k-1)c^*}}$$

$$\times \sigma^{-\alpha} G_{kp+lv, kq+lu}^{km+lt, kn+ls} \left(\frac{\omega^k k^k (\rho - q)}{\sigma^l \Gamma(u-v)} \left| \begin{matrix} \frac{a_1}{k}, \dots, \frac{a_1+k-1}{k}, \dots, \frac{a_n}{k}, \dots, \frac{a_n+k-1}{k}, \frac{1-\alpha-d_1}{l}, \dots, \frac{l-\alpha-d_1}{l}, \dots, \frac{1-\alpha-d_s}{l}, \dots, \frac{l-\alpha-d_s}{l}, \frac{1-\alpha-d_{s+1}}{l}, \dots, \frac{l-\alpha-d_{s+1}}{l} \\ \frac{b_1}{k}, \dots, \frac{b_1+k-1}{k}, \dots, \frac{b_m}{k}, \dots, \frac{b_m+k-1}{k}, \frac{1-\alpha-c_1}{l}, \dots, \frac{l-\alpha-c_1}{l}, \dots, \frac{1-\alpha-c_t}{l}, \dots, \frac{l-\alpha-c_t}{l}, \frac{1-\alpha-c_{t+1}}{l}, \dots, \frac{l-\alpha-c_{t+1}}{l} \end{matrix} \right. \right) \tag{39}$$

where

$$\begin{aligned}
 b^* &= s + t - \frac{u + v}{2} \\
 c^* &= m + n - \frac{p + q}{2} \\
 \rho &= \sum_{j=1}^v d_j - \sum_{j=1}^u c_j + \frac{u - v}{2} + 1 \\
 \mu &= \sum_{j=1}^q b_j - \sum_{j=1}^p a_j + \frac{p - q}{2} + 1
 \end{aligned} \tag{40}$$

References

- [1] I. S. Ansari, M. M. Abdallah, M. S. Alouini, and K. A. Qaraqe, "Outage performance analysis of underlay cognitive RF and FSO wireless channels," in *Proc. 3rd Int. Workshop Opt. Wireless Commun.*, Funchal, Madeira Island, Portugal, Sep. 2014, pp. 6–10.
- [2] H. K. Al-Musawi *et al.*, "Adaptation of mode filtering technique in 4G-LTE hybrid RoMMF-FSO for last-mile access network," *J. Lightw. Technol.*, vol. 35, no. 17, pp. 3758–3764, Sep. 2017.
- [3] T. A. Tsiftsis, H. G. Sandalidis, G. K. Karagiannidis, and N. C. Sagias, "Multihop free-space optical communications over strong turbulence channels," in *Proc. IEEE Int. Conf. Commun.*, vol. 6, Istanbul, Turkey, Jun. 2006, pp. 2755–2759.
- [4] S. S. Muhammad, T. Javorik, I. Jelovcan, Z. Ghassemlooy, and E. Leitgeb, "Comparison of hard-decision and soft-decision channel coded M-ary PPM performance over free space optical links," *Eur. Trans. Telecommun.*, vol. 20, pp. 746–757, Nov. 2008.
- [5] W. Gappmair and S. S. Muhammad, "Error performance of terrestrial FSO links modelled as PPM/poisson channels in turbulent atmosphere," *Electron. Lett.*, vol. 43, no. 5, pp. 63–64, Mar. 2007.
- [6] W. Gappmair and H. E. Nistazakis, "Subcarrier PSK performance in terrestrial FSO links impaired by gamma-gamma fading, pointing errors, and phase noise," *J. Lightw. Technol.*, vol. 35, no. 9, pp. 1624–1632, May 2017.
- [7] W. Lim, C. Tae-Sik, C. Yun, and K. Kim, "BER performance of coherent DPSK free-space optical systems with APD over turbulence channels," in *Proc. 14th OptoElectron. Commun. Conf.*, Hong Kong, China, Jul. 2009, pp. 1–2.
- [8] H. T. T. Pham, P. V. Trinh, D. N. T., and A. T. Pham, "A comprehensive performance analysis of PPM-based FSO systems with APD receiver in atmospheric turbulence," in *Proc. Int. Conf. Adv. Technol. Commun.*, Hanoi, Vietnam, Oct. 2012, pp. 357–361.
- [9] E. Farooq, S. K. Gupta, and A. Sahu, "BER analysis of OOK and DPSK schemes in gamma-gamma turbulence channel with PIN and APD photodetector," in *Proc. 8th Int. Conf. Comput. Commun. Netw. Technol.*, IIT Delhi, India, Jul. 2017, pp. 1–4.
- [10] R. L. Al-habash, M. A. Andrews, and L. C. Phillips, "Mathematical model for the irradiance probability density function of a laser beam propagating through turbulent media," *Opt. Eng.*, vol. 40, pp. 1554–1562, Aug. 2001.
- [11] X. M. Zhu and J. M. Kahn, "Free-space optical communication through atmospheric turbulence channels," *IEEE Trans. Commun.*, vol. 50, no. 8, pp. 1293–1300, Aug. 2002.
- [12] J. C. Campbell, "Recent advances in telecommunications avalanche photodiodes," *J. Lightw. Technol.*, vol. 25, no. 1, pp. 109–121, Jan. 2007.
- [13] K. Kiasaleh, "Receiver architecture for channel-aided, OOK, APD-based FSO communications through turbulent atmosphere," *IEEE Trans. Commun.*, vol. 63, no. 1, pp. 186–194, Jan. 2015.
- [14] K. Kiasaleh, "Performance of APD-based, PPM free-space optical communication systems in atmospheric turbulence," *IEEE Trans. Commun.*, vol. 53, no. 9, pp. 1455–1461, Sep. 2005.
- [15] R. M. Gagliardi and S. Karp, *Optical Communications*. New York, NY, USA: Wiley, 1995.
- [16] M. K. Simon and M. S. Alouini, *Digital Communication Over Fading Channels*. New York, NY, USA: Wiley, 2000.
- [17] V. S. Adamchik and O. I. Marichev, "The algorithm for calculating integrals of hypergeometric type function and its realization in reduce system," in *Proc. Int. Symp. Symbolic Algebr. Comput.*, Tokyo, Japan, Jul. 1990, pp. 212–224.
- [18] Wolfram function site, series representation of Meijer G-functions, Feb. 2018. [Online]. Available: <http://wolfram.com>
- [19] W. Lim, "BER analysis of coherent free space optical systems with BPSK over gamma-gamma channels," *J. Opt. Soc. Korea*, vol. 19, no. 3, pp. 237–240, Jun. 2015.
- [20] Y. Tang and M. Brandt-Pearce, "Link allocation, routing, and scheduling for hybrid FSO/RF wireless mesh networks," *IEEE/OSA J. Opt. Commun. Netw.*, vol. 6, no. 1, pp. 86–95, Jan. 2014.
- [21] D. A. Luong, C. T. Truong, and A. T. Pham, "Effect of APD and thermal noises on the performance of SC-BPSK/FSO systems over turbulence channels," in *Proc. 18th Asia-Pacif. Conf. Commun.*, Jeju, South Korea, Oct. 2012, pp. 344–349.
- [22] S. S. Muhammad, W. Gappmair, and E. Leitgeb, "PPM channel capacity evaluation for terrestrial FSO links," in *Proc. Int. Workshop Satell. Space Commun.*, Madrid, Spain, Sep. 2006, pp. 222–226.
- [23] H. E. Nistazakis, T. A. Tsiftsis, and G. S. Tombras, "Performance analysis of free-space optical communication systems over atmospheric turbulence channels," *IET Commun.*, vol. 3, no. 8, pp. 1402–1409, Aug. 2009.
- [24] W. Gappmair, "Further results on the capacity of free-space optical channels in turbulent atmosphere," *IET Commun.*, vol. 5, no. 9, pp. 1262–1267, Jun. 2011.
- [25] S. Jagtar and V. K. Jain, "Performance analysis of BPPM and M-ary PPM optical communication systems in atmospheric turbulence," *IETE Tech. Rev.*, vol. 25, no. 4, pp. 146–153, Sep. 2008.